# Multifractal Nature of the Dissipation Field of Passive Scalars in Fully Turbulent Flows

R. R. Prasad, C. Meneveau, and K. R. Sreenivasan

*Mason Laboratory, Yale University, New Haven, Connecticut 06520*

We present measurements of the curve of $f$ vs $\alpha$ from two-dimensional sections of the "dissipation" field of concentration fluctuations, and from one-dimensional sections of the dissipation field of passive temperature fluctuations, in turbulent jets. The results confirm the universality of the dissipation rate $\chi$ of scalar fluctuations and the applicability of Taylor's hypothesis, and show that the curve of $f$ vs $\alpha$ is the same for different components of $\chi$, that the additive properties of $f(\alpha)$ apply to intersections, and that the intermittency exponent of $\chi$ is considerably higher than that for the turbulent kinetic-energy dissipation.

It has been recognized[1-3] that intermittent quantities or measures naturally lend themselves to be characterized as multifractals. In this picture, local singularities of different strengths $\alpha$ are distributed on interwoven sets of varying dimensionality $f(\alpha)$, while moments of order $q$ obey power laws involving the so-called generalized dimensions[4] $D_q$. For a general review, see Refs. 1-4, and Meneveau and Sreenivasan.[5] These ideas have been applied to turbulence[1,2,5-7] and the curves of $D_q$ vs $q$ and $f$ vs $\alpha$ for the dissipation of turbulent kinetic energy, $\epsilon$, have been measured,[5] and shown to be universal features of fully developed turbulence. Another quantity of practical interest is the "dissipation" of passive scalar fluctuations $\chi = \Gamma (\partial \theta / \partial x_i)^2$, where $x_i$ represent spatial coordinates and $\theta$ is a passive scalar (e.g., concentration $C$ of a contaminant or temperature $T$), and $\Gamma$ the corresponding molecular diffusivity. $\chi$ does not involve cross terms, and contains only three components (of which we measure two) instead of nine components in $\epsilon$ (of which only one component was measured[5]). Extensive measurements of $\chi$ have been made[8,9] for the case when the passive scalar is the temperature, and the results on the probability densities[9] as well as the scaling properties of the temperature structure functions[10] were shown to be at variance with a log-normal[11] distribution, as well as with the $\beta$ model.[12] In conformity with our previous findings on $\epsilon$, it seems natural to conjecture that $\chi$ is distributed according to a multifractal distribution, i.e., $\chi_r$, the local average of $\chi$ over a domain of size $r$ centered at $\mathbf{x}$, obeys a power law $\chi_r \sim r^{\alpha - 1}$, $\alpha$ being a function of $\mathbf{x}$. This Letter describes measurements of the curves of $D_q$ vs $q$ and $f$ vs $\alpha$ for $\chi$ using both one- and two-dimensional slicing of the three-dimensional scalar dissipation field, and presents conclusions related to questions of isotropy, intersections of $\chi$ with lower-dimensional subspaces, and intermittency.

For two-dimensional slicing, the concentration $C$ of a contaminant was used as the passive scalar. A water jet seeded with sodium fluorescein dye flowing into a tank of quiescent water was illuminated by a sheet of a pulsed laser light of thickness 200–250 $\mu$m and duration 8 ns. The diameter $D$ of the nozzle was 12 mm and the exit velocity $U$ was 0.3 m/s. These conditions lead to a Landau-type estimate of about 330 for the ratio of the large scale $L$ to the Kolmogorov scale $\eta$, and an $\eta$ itself of about 250 $\mu$m. Images of the "instantaneous" turbulent concentration field (proportional to the intensity of laser-induced fluorescence) were obtained with a charge-coupled-device camera consisting of $1400 \times 1035$ pixels, and digitized with twelve-bit resolution. Figure 1
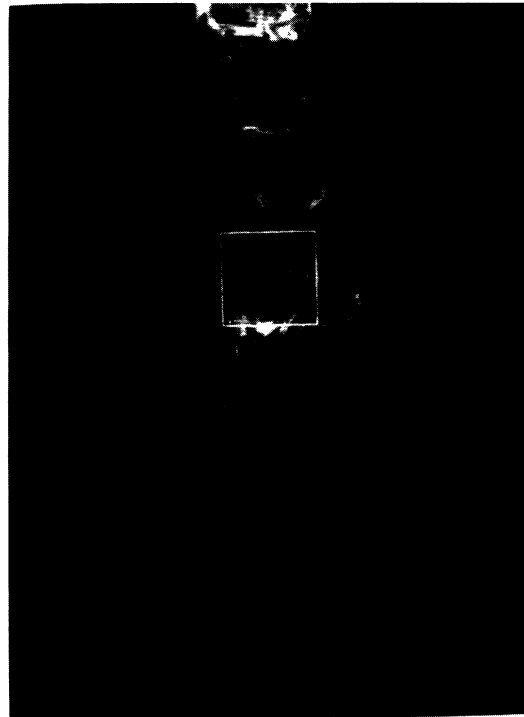


FIG. 1. Digitized image of the concentration field in a turbulent water jet, illuminated by a thin laser sheet. The box shows a region typically used for the calculations, which is fully contained within the jet fluid (see text).
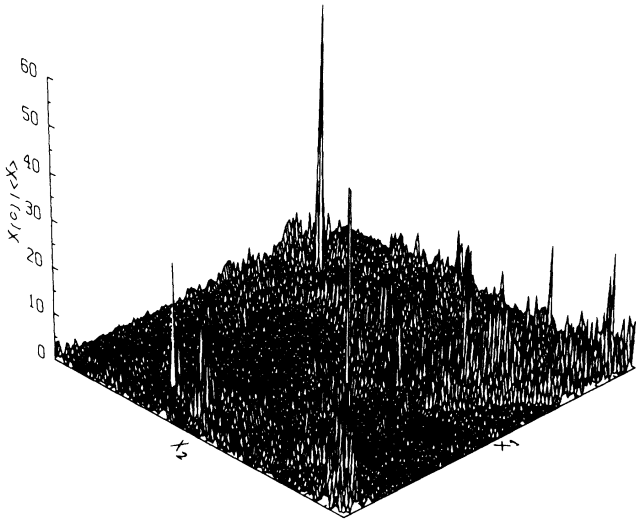
    © 1988 The American Physical Society

FIG. 2. Dissipation of concentration fluctuations $\chi(C)/\langle\chi\rangle$ as a function of $x_1$ and $x_2$, within the box of Fig. 1.

shows an image, which is an instantaneous graph of $C$ as a function of two spatial coordinates $x_1$ and $x_2$, $x_1$ being the streamwise direction. Also shown is a square region of $150 \times 150$ pixels that is *fully contained within the turbulent jet*. All computations explained below were made in such regions.

As mentioned earlier, the quantity $\chi(C)$ consists of the three terms:

$$\chi(C) = \Gamma[(\partial C/\partial x_1)^2 + (\partial C/\partial x_2)^2 + (\partial C/\partial x_3)^2].$$

Two of these terms are accessible from the digitized images by differentiation of $C$ with respect to $x_1$ and $x_2$. Figure 2 shows $\chi(C)$ (divided by its average $\langle\chi\rangle$) calculated with those two terms within the square region shown in Fig. 1. The high intermittency and qualitative resemblance to multifractional measures is immediate.

In order to make quantitative statements about the distribution of $\chi(C)$, the set of generalized dimensions $D_q$ was obtained by division of an appropriately chosen interior jet region into smaller square regions of size $r$, and by the identification of the power laws[3-5] of the type

$$\sum (X_r/X_L)^q \sim r^{(q-1)D_q}. \tag{1}$$

Here $X_r$ is the integral of $\chi(C)$ over a box of size $r$, $X_L$ is the total dissipation, and the sum is taken over all squares of size $r$ contained in the domain. This is repeated for twelve different values of $r$ ranging from 1 pixel, corresponding roughly to $r = \eta$, up to $r = 150$ pixels. According to Eq. (1), if log-log plots of $[\sum (X_r/X_L)^q]^{1/(q-1)}$ vs $r$ present linear regions for $r$ within the scaling range (observed in Ref. 5 to be $\eta \lesssim r \lesssim L$), then the slopes correspond to $D_q$. When the regions used to measure the "generalized dimensions" were completely inside the turbulent jet (as in Fig. 1), straight lines were observed for close to 2 decades from $r = 1$ pixel to $r \approx 80$ pixels, per-
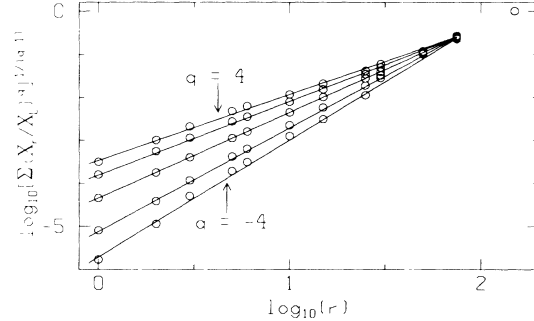


FIG. 3. Typical log-log plots of $[\sum (X_r/X_L)^q]^{1/(q-1)}$ vs $r$ for $q = -4, -2, 0, 2,$ and 4.

mitting accurate determination of $D_q$ (see Fig. 3). Jet regions which were not entirely turbulent were not used, because the interpretation of such results is not clear: Recalling that the dye interface is a fractal,[13] we then have a multifractal measure bounded by a fractal interface—a more complex object. For such regions, no convincing scaling was observed for $q < 0$. This will be discussed elsewhere.

From the $D_q$ curves obtained, the $f(\alpha)$ curves were computed with the Legendre transforms[5] (with $d = 2$ for two-dimensional sections of the flow)

$$\alpha = (d/dq)[(q-1)D_q] + 1 - d, \tag{2a}$$

$$f(\alpha) = q(\alpha - 1 + d) - (q-1)D_q. \tag{2b}$$

Figure 4 shows the $f$ vs $\alpha$ curves for five different regions in different realizations of the flow. The continuous curve represents the $f$ vs $\alpha$ curve obtained with Eqs. (2) on the averaged $D_q$ curve. The scatter of the data is
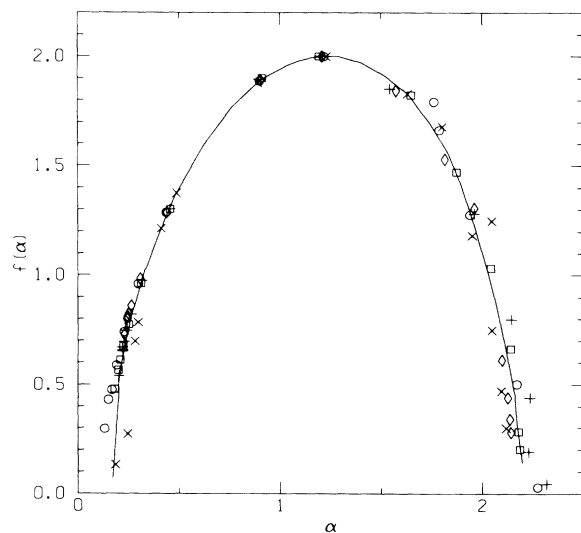


FIG. 4. $f$ vs $\alpha$ curves obtained from five different regions like Fig. 2. The continuous curve is the $f$ vs $\alpha$ curve obtained from the averaged $D_q$ curve.
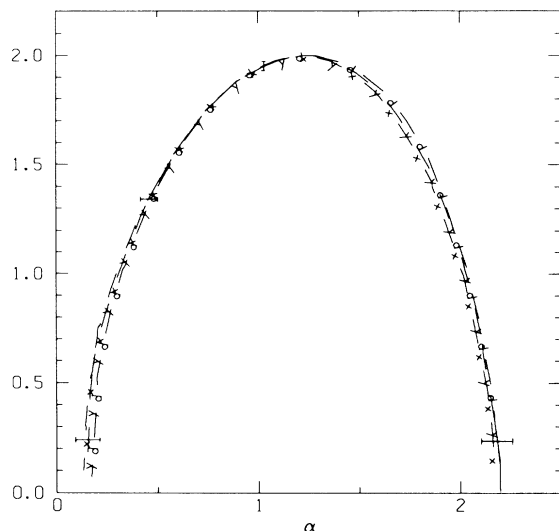
FIG. 5. Comparison of average $f$ vs $\alpha$ curve for $\chi \sim (\partial C/\partial x_1)^2$ (the $x$ curve), $\chi \sim (\partial C/\partial x_2)^2$ (the $y$ curve), and $\chi \sim (\partial C/\partial x_1)^2 + (\partial C/\partial x_2)^2$ (the $d$ curve).
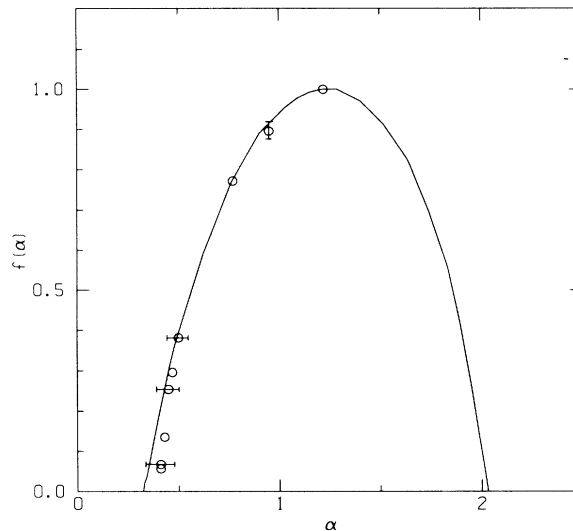


FIG. 6. Average $f$ vs $\alpha$ curve for one-dimensional sections through $\chi(T)$ (circles) and variability observed from one data set to another (error bars). Only the portion of the curve corresponding to $q \geq 0$ is shown. The continuous corresponds to the $f$ vs $\alpha$ curve of $\chi(C)$ minus 1 (see text).

small, much lower than for one-dimensional sections of $\epsilon$.

Notice that we did not include the last component $(\partial C/\partial x_3)^2$ in the calculation of $\chi(C)$. In doing so, we assumed that the $f$ vs $\alpha$ curve of any one term $(\partial C/\partial x_i)^2$ could not differ appreciably from that of the others or of the sum. This assumption about their scaling behavior has been checked by comparing the $f$ vs $\alpha$ curves obtained separately from $(\partial C/\partial x_1)^2$ and $(\partial C/\partial x_2)^2$. The averages and variability of five realizations are shown in Fig. 5. It is seen that they agree very well within experimental scatter, confirming the hypothesis of small-scale isotropy used to obtain $\chi(C)$. This small-scale isotropy refers to the equality of power-law exponents of the different components of $\chi$, and not to their absolute values. The present results do not rule out different preexponential factors in all relevant scaling laws for different components[9] of $\chi$.

Next, the $f$ vs $\alpha$ curve for one-dimensional sections was obtained. The passive scalar used in this context was the temperature, and the flow was a heated air jet ($D = 2.5$ cm, $U = 5$ m/s). Measurements were made at an axial distance $x_1/D = 25$ from the nozzle and on the fluid-dynamic center line of the jet where the temperature rise above the ambient was $5\,^\circ$C. The temperature was measured with a cold wire (diameter $= 0.63$ $\mu$m) operated at a constant current of 90 $\mu$A in order to minimize the influence of flow velocity. Following Ref. 5, the time trace of temperature was interpreted as a one-dimensional spatial cut through the flow field in the streamwise direction $x_1$ with Taylor's frozen-flow hypothesis. The dissipation of temperature fluctuations was calculated with only one component $\chi(T) \sim (\partial T/$

$\partial x_1)^2$ which, on the basis of Fig. 5, seems reasonable. The $D_q$ curve was obtained with Eq. (1), where $X_r$ is now the integral of $\chi(T)$ within a segment of length $r$. This was repeated for 30 signals each of which was $40L$ long, and the resulting values of $D_q$ were averaged. (For a detailed description of the experimental pointers to measuring $D_q$ curves and selecting the length of the signals to be analyzed, see Ref. 5.) Since the uncertainty in the determination of $D_q$ for $q < 0$ was relatively high (this being due to noise, which reduces the scaling range for negative $q$, as explained in Appendix C of Ref. 5), only the results for $q \geq 0$ are presented. Finally, Eqs. (2) with $d = 1$ were used on the averaged $D_q$ curve to obtain the $f$ vs $\alpha$ curve for the one-dimensional cuts through $\chi(T)$. The results, corresponding to the left side of the $f$ vs $\alpha$ curve, are shown as circles in Fig. 6, along with typical experimental variability.

A comparison of results from one- and two-dimensional sections can now be made. With the understanding that fractal dimensions follow additive laws under intersections—see Mandelbrot[14] and references cited there—it is expected that the $f$ vs $\alpha$ curve of the one-dimensional sections will be one less than that of the two-dimensional section. The line in Fig. 6 corresponds to $f(\alpha) - 1$ vs $\alpha$ for the case of $\chi(C)$, obtained by the subtraction of unity from the continuous curve of Fig. 4. This was done only by an interval of $\alpha$ such that $f(\alpha) - 1 \geq 0$. The agreement between the two curves is good within experimental uncertainty.

Since the results of one- and two-dimensional slicing agree, the interpretation of a temporal signal as a one-

dimensional spatial cut appears plausible in the present context. Also, the Schmidt number in the two cases differs greatly (by a factor of 1000 or more), and the Reynolds number was also quite different. This is an indication that the present results are universal characteristics of the dissipation of passive scalar fluctuations, independent of the scalar, provided that it is passive and that the Reynolds number is sufficiently high.

A last remark concerning the intermittency of $\chi$ should be made. From Fig. 5 it is seen (for one-dimensional cuts) that $\alpha_{min} = 0.40 \pm 0.07$, which is lower than $\alpha_{min}$ observed for $\epsilon$ ($\alpha_{min} = 0.51 \pm 0.05$). This means that $\chi$ has stronger singularities than $\epsilon$. Also, noting[5] that the intermittency exponent $\mu$ is given in terms of the $D_q$ curve as $\mu = -2dD_q/dq$, or equivalently as $\mu = 2[\alpha - 1 + d - f(\alpha)]$, both evaluated at $q = 0$, one obtains $\mu_\chi = 0.38 \pm 0.08$, higher than the intermittency exponent of $\epsilon$ ($\mu_\epsilon = 0.25 \pm 0.05$). This agrees with experimental results[9] obtained with Kolmogorov's relation between the variance of $\log(\chi_r)$ and $\log(\epsilon_r)$ vs $\log(L/r)$.

---

[1] B. B. Mandelbrot, J. Fluid Mech. 62, 331 (1974).

[2] U. Frisch and G. Parisi, in Turbulence and Predictability in Geophysical Fluid Dynamics and Climate Dynamics, edited by M. Ghil, R. Benzi, and G. Parisi (North-Holland, New York, 1985), p. 84.

[3] T. C. Halsey, M. H. Jensen, L. P. Kadanoff, I. Procaccia, and B. I. Shraiman, Phys. Rev. A 33, 1141 (1986).

[4] H. G. E. Hentschel and I. Procaccia, Physica (Amsterdam) 8D, 435 (1983).

[5] C. Meneveau and K. R. Sreenivasan, in The Physics of Chaos and Systems Far from Equilibrium, edited by Minh-Duong Van [Nucl. Phys. B, Proc. Suppl. 2, p. 49 (1987)].

[6] C. Meneveau and K. R. Sreenivasan, Phys. Rev. Lett. 59, 1424 (1987).

[7] R. Benzi, G. Paladin, G. Parisi, and A. Vulpiani, J. Phys. A 17, 3521 (1984).

[8] C. H. Gibson, G. R. Stegen, and R. B. Williams, J. Fluid Mech. 41, 153 (1970).

[9] K. R. Sreenivasan, R. A. Antonia, and H. Q. Danh, Phys. Fluids 20, 1238 (1977).

[10] R. A. Antonia, E. J. Hopfinger, Y. Gagne, and F. Anselmet, Phys. Rev. A 30, 2704 (1984).

[11] A. N. Kolmogorov, J. Fluid Mech. 13, 82 (1962).

[12] U. Frisch, P. L. Sulem, and M. Nelkin, J. Fluid Mech. 87, 719 (1978).

[13] K. R. Sreenivasan and C. Meneveau, J. Fluid Mech. 173, 357 (1986); K. R. Sreenivasan, R. R. Prasad, C. Meneveau, and R. Ramshankar, in "Fractals in Geophysics," edited by C. Scholz and B. Mandelbrot (Birkhauser, Therwil, Switzerland, to be published).

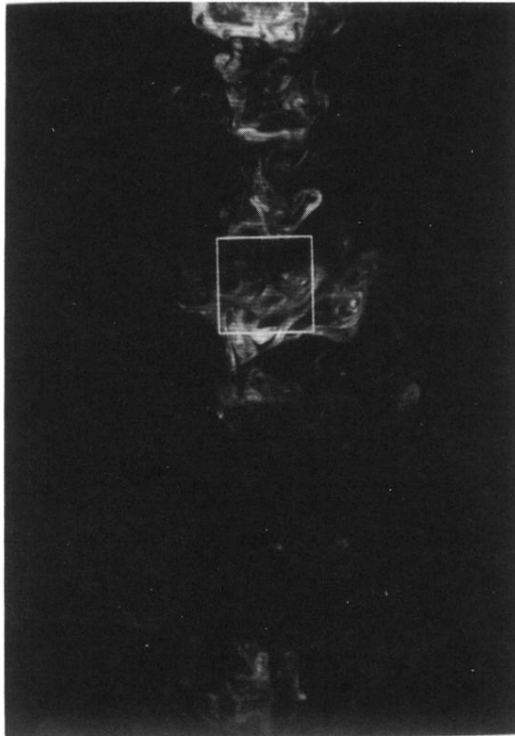[14] B. B. Mandelbrot, The Fractal Geometry of Nature (Freeman, San Fransisco, 1982).

FIG. 1. Digitized image of the concentration field in a turbulent water jet, illuminated by a thin laser sheet. The box shows a region typically used for the calculations, which is fully contained within the jet fluid (see text).
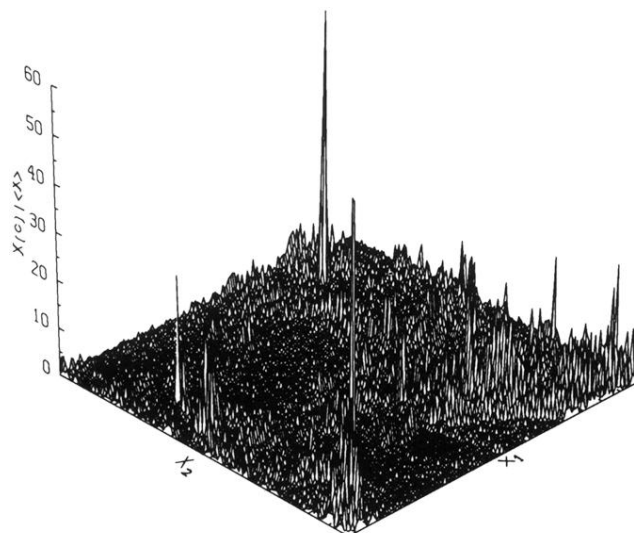
FIG. 2. Dissipation of concentration fluctuations $\chi(C)/\langle\chi\rangle$ as a function of $x_1$ and $x_2$, within the box of Fig. 1.